

Layered Double Hydroxide Nanocomposite Coatings for Improved Flame Retardancy of Polyethylene-Based Copolymers

Original

Layered Double Hydroxide Nanocomposite Coatings for Improved Flame Retardancy of Polyethylene-Based Copolymers / Trapani, G., Arrigo, R., Sisani, M., Bastianini, M., Frache, A.. - In: POLYMERS. - ISSN 2073-4360. - 17:23(2025), pp. 1-12. [10.3390/polym17233189]

Availability:

This version is available at: 11583/3005600 since: 2025-12-02T16:41:00Z

Publisher:

MDPI

Published

DOI:10.3390/polym17233189

Terms of use:

This article is made available under terms and conditions as specified in the corresponding bibliographic description in the repository

Publisher copyright

(Article begins on next page)

Article

Layered Double Hydroxide Nanocomposite Coatings for Improved Flame Retardancy of Polyethylene-Based Copolymers

Giuseppe Trapani ¹, Rossella Arrigo ¹, Michele Sisani ², Maria Bastianini ² and Alberto Frache ^{1,*}

¹ Department of Applied Science and Technology, Politecnico di Torino, Viale Teresa Michel 5, 15121 Alessandria, Italy; giuseppe.trapani@polito.it (G.T.); rossella.arrigo@polito.it (R.A.)

² Prolabin&Tefarm, Ponte Felicino, 06134 Perugia, Italy; michele.sisani@prolabintefarm.com (M.S.); maria.bastianini@prolabintefarm.com (M.B.)

* Correspondence: alberto.frache@polito.it

Abstract

This work proposes a coating approach for obtaining flame-retardant ethylene–vinyl acetate (EVA) and ethylene–butyl acrylate (EBA) copolymer-based materials. Nanocomposite films of EVA and EBA were first produced by cast extrusion, with two types of layered double hydroxides (LDHs) differing in the aspect ratio used as nanofillers. Subsequently, the films were applied as a coating to the corresponding neat copolymer substrate, and the combustion behavior of the so-obtained samples was evaluated through cone calorimeter tests. Despite the small amount of nanofillers (0.5 wt.% considering the whole specimen), the application of the coatings significantly improved the time to ignition compared to the pristine copolymers, while the shape of the heat release rate curves and the relative peak values remained relatively unchanged. The effect of the embedded nanofillers in delaying the ignition was more effective for the EVA-based systems than for the EBA ones (showing an increment of 30% and 12%, respectively, compared to the uncoated samples), likely due to the more homogeneous dispersion of the LDHs obtained in the first case. The obtained results demonstrate the effectiveness of the coating approach, since it allows the flame-retardant action to be concentrated on the surface of a polymer system, where combustion specifically takes place, while minimizing the required amount of flame retardant.

Keywords: ethylene–vinyl acetate; ethylene–butyl acrylate; cast extrusion; cone calorimeter; combustion behavior



Academic Editor: Jun Sun

Received: 30 October 2025

Revised: 27 November 2025

Accepted: 28 November 2025

Published: 29 November 2025

Citation: Trapani, G.; Arrigo, R.; Sisani, M.; Bastianini, M.; Frache, A. Layered Double Hydroxide Nanocomposite Coatings for Improved Flame Retardancy of Polyethylene-Based Copolymers. *Polymers* **2025**, *17*, 3189. <https://doi.org/10.3390/polym17233189>

Copyright: © 2025 by the authors. Licensee MDPI, Basel, Switzerland. This article is an open access article distributed under the terms and conditions of the Creative Commons Attribution (CC BY) license (<https://creativecommons.org/licenses/by/4.0/>).

1. Introduction

Thermoplastic polymers are renowned for several key characteristics, such as their easy processability, low cost compared to other materials, lightweight, and versatility. However, one of the most severe issues of these materials is undoubtedly their high flammability [1] and all the consequent concerns in terms of risk to the health and life of people involved in fires and the pollution produced by the resulting fumes. Various approaches have been developed to overcome these issues, from the chemical functionalization of polymer chains [2] to additives and fillers being introduced through a compounding step. The most commonly employed flame-retardant additives include metal hydroxides [3], halogenates [4,5], phosphorus compounds [6], intumescent systems [7,8], and nanoparticles [9,10], with the possibility of exploiting the synergy between different systems [11,12].

Ethylene–vinyl acetate (EVA) and ethylene–butyl acrylate (EBA) copolymers are commodities that are widely utilized in the fabrication of sheaths for electrical cables, pipes, and films. These materials are therefore employed in a range of applications where the

flame-retardant properties of the materials are required [13]. Concerning EVA, there is a large number of studies in the literature dealing with the development of several strategies for improving its flame retardancy through the introduction of additives and/or fillers in the bulk [14–18]. For instance, Camino et al. [19] compared the behavior of EVA-based systems containing a layered double hydroxide (LDH), magnesium hydroxide, aluminum hydroxide, or boehmite, demonstrating that the utilization of hydrotalcites caused a significant decrease in the time to ignition compared to the pristine matrix. Furthermore, it was shown that, similarly to conventional magnesium and aluminum hydroxides [20,21], the water molecules trapped in between the LDH layers can dilute the flammable gases during pyrolysis, thus inhibiting flame propagation in burning materials. Additionally, in the same work, it is reported that LDHs are also able to form a mixed oxide residue that leads to an insulating char layer acting as additional protection for the underlying polymer. In contrast, for EBA, there are only a few works discussing approaches for flame retardancy [22,23]. This copolymer, however, can be considered a superior alternative to EVA, given its reduced polarity, attributable to the length of the butyl groups compared to the acetate ones of EVA. This lower polarity results in reduced hygroscopic tendency [24], a property that can be pivotal in specific applications, such as cable sheathing.

Regardless of the specific polymer, the most prevalent approach to flame retardancy entails the incorporation of high concentrations (typically a minimum of 50 wt%) of flame-retardant additives. This strategy, however, gives rise to two direct consequences. Firstly, it is evident that the mechanical properties of the material are subject to a complete alteration. In the case of EVA and EBA, there is an evident transition from a flexible to a significantly more rigid and brittle behavior [19], which is not generally desirable, particularly in applications such as wire coatings, where flexibility is an essential attribute that must be preserved. On the other hand, the incorporation of high loadings of inorganic fillers has been demonstrated to result in a significant alteration in the average density of the material. This, in turn, has a significant impact on the overall weight of the final object [25]. In order to circumvent these issues, an alternative approach has been proposed, namely the localization of flame retardants on the surface of the polymer, where combustion specifically takes place. In this context, Colonna et al. [26] demonstrated that the time to ignition of an EVA-based system containing organomodified nanoclays can be significantly enhanced through an aging treatment at a temperature close to the melting point, which promotes an easier migration of the clay toward the surface during the early stage of combustion. The strategy of exploiting protective coatings for flame retardancy has been extensively reviewed by Malucelli et al. [27], showing that the presence of a coating on the polymer surface, capable of regulating the heat and mass flows, allows the fire behavior of the material to be governed. Additionally, Matta et al. [28] showed that the localization of the flame retardant on the polymer surface promotes an initial shielding effect that causes a postponement in the time to ignition and the time to peak.

In this work, nanostructured films based on EVA and EBA and containing two types of LDHs characterized by different dimensions were formulated through cast extrusion and applied as coatings on unfilled substrates. The aim was to assess their influence on the combustion behavior of the two copolymers. After a preliminary characterization of the films' microstructure, coated specimens were produced and subjected to cone calorimeter tests. The obtained results highlighted an increase in the time to ignition compared to the uncoated samples, especially for the EVA-based systems, confirming the effectiveness of the proposed method to improve fire safety.

2. Materials and Methods

2.1. Materials

The polymers used in this work as matrices were (i) ethylene–butyl acrylate (EBA) Lucofin[®] 1400MN (supplied by Lucobit, Wesseling, Germany), with a butyl acrylate content of 17%, and (ii) ethylene–vinyl acetate (EVA) Greenflex MQ 40 BA (by Versalis, San Donato Milanese, Italy), with a vinyl acetate content of 19%. Both copolymers are characterized by a melt flow index of 7.0 g/10 min (190 °C, 2.16 kg).

Two types of layered double hydroxides (LDHs) with different dimensions and modified with oleate groups ($[\text{Mg}_{0.66}\text{Al}_{0.34}(\text{OH})_2](\text{C}_{18}\text{H}_{35}\text{O}_2)_{0.34} \times 0.9 \text{H}_2\text{O}$) were used, both synthesized by Prolabin&Tefarm (Perugia, Italy). Hereinafter, the LDHs are referred to as S-LDHs ($D_{50} = 5.60 \mu\text{m}$, $D_{90} = 28.78 \mu\text{m}$) and L-LDHs ($D_{50} = 18.67 \mu\text{m}$, $D_{90} = 48.91 \mu\text{m}$).

2.2. Processing and Sample Preparation

The EBA- and EVA-based nanocomposite films were produced through melt compounding and cast extrusion using a twin-screw extruder Thermo Fisher Scientific[™] Process 11 (Waltham, MA, USA) equipped with a rectangular-shaped die (thickness = 1 mm, width = 25 mm) and a Process 11 Sheet Take Off Unit (Thermo Fisher Scientific[™] Waltham, MA, USA). The selected processing conditions were as follows: screw rotation speed of 150 rpm, feed rate of 500 g/h, and temperature profile of 160-165-170-180-190-190-190 °C and 140-160-170-180-180-180-180 °C for EBA- and EVA-based materials, respectively.

The so-produced nanocomposite films (LDH content: 5 wt%) were characterized by a thickness of about 280 μm .

A Collins (Maitenbeth, Germany) P200T hot plate press, operating at 190 °C and 100 bar, was used to produce 50 × 50 × 3 pristine copolymer specimens, which were used as substrates to produce coated samples and as a reference for all the characterizations. To this aim, the films obtained via cast extrusion were applied to the compression-molded specimens of pristine EBA and EVA through a further compression molding process using a Collins (Maitenbeth, Germany) P200T hot plate press at 85 °C and 20 bar for 30 s.

2.3. Characterization Techniques

Thermogravimetric analyses were performed on samples of 10 ± 1 mg using a Discovery TGA 5500 (TA Instrument, New Castle, DE, USA); the samples were heated from 50 to 700 °C at 10 °C/min under air flow (25 mL/min). T_{onset} (temperature at which 2% of weight loss occurs) and T_{max} (temperature at which maximum weight loss rate is observed in dTG (derivative) curves) were evaluated.

The thermal characterization of the coating films was performed using a DSC TA Q20 (TA Instruments, New Castle, DE, USA) with the following thermal cycle (performed under a nitrogen atmosphere): a first heating scan from −70 °C to 200 °C, an isothermal step at 200 °C for 3 min, a cooling scan from 200 °C to −70 °C, and a second heating ramp from −70 °C to 200 °C. During all the steps, the rate of heating/cooling was maintained at 10 °C/min. The melting temperature (T_m) and the melting enthalpy (ΔH_m) of all the samples were evaluated in the first heating scan. Additionally, the crystallinity content (χ_c) was evaluated, taking into account that EBA and EVA are polyethylene-based copolymers in which only the polyethylene fraction is able to crystallize, while butyl acrylate and vinyl acetate fractions are amorphous. χ_c was calculated using the following formula:

$$\chi_c = \frac{\Delta H_m}{PE\% \cdot \Delta H_m^0 \cdot (1 - x)} \cdot 100 \quad (1)$$

where ΔH_m is the melting enthalpy, $PE\%$ is the polyethylene content of EBA and EVA (0.83 and 0.81, respectively), ΔH_m^0 is the melting enthalpy of the 100% crystalline polyethylene (277 J/g [28]), and x represents the nanofiller content.

The rheological behavior of the unfilled and nanocomposite films was evaluated in an inert atmosphere (N_2) using an ARES (TA Instruments, New Castle, DE, USA) strain-controlled plate–plate rheometer. Frequency sweep measurements were performed at 190 or 180 °C for EBA- or EVA-based materials, respectively. For the unfilled films, the tests were carried out from 100 to 0.1 rad/s, while a frequency range of 100–0.01 rad/s was selected for the nanocomposites. The strain amplitude was selected for each sample to fall in the linear viscoelastic region (preliminary assessed through strain sweep tests). The complex viscosity data as a function of the frequency were fitted using the following Cross-like model modified to take into account the yield stress [29]:

$$\eta^*(\omega) = \frac{\eta_0}{[1 + (\lambda\omega)^{1-n}]^{1/n}} + \frac{\sigma_0}{\omega} \quad (2)$$

where η^* is the complex viscosity, ω is the frequency, η_0 is the zero-shear viscosity, λ is the relaxation time, n is the flow index, and σ_0 is the yield stress.

A Zeiss (Oberkochen, Germany) EVO 15 Scanning Electron Microscope (SEM) (20 kV beam voltage and 8.5 mm working distance) was used for morphological analysis. The sections to be observed were obtained by fracturing the films (in the direction parallel to the machine direction) in liquid nitrogen. The samples were gold sputtered prior to morphological analysis.

The combustion behavior was evaluated with a Noselab ATS (Monza, Italy) cone calorimeter, according to the ISO5660 standard. EBA-based specimens were tested under a radiant heat flux of 25 and 30 kW/m², while for EVA-based materials, a heat flux of 30 kW/m² was used. To ensure reliability, three replicates were performed for each system, allowing for the estimation of the time to ignition (TTI), the heat release rate (HRR), the total heat release (THR), the peak of the heat release rate (pkHRR), and the time of the pkHRR (t_{peak}). In addition, to evaluate the fire hazard, the fire growth rate index (FIGRA) was calculated according to Equation (3) [30], while for the fire performance index (FPI), Equation (4) was used [31]:

$$FIGRA = \frac{pkHRR}{t_{peak}} \quad (3)$$

$$FPI = \frac{TTI}{pkHRR} \quad (4)$$

3. Results

3.1. Preliminary Characterization of EVA- and EBA-Based Nanocomposite Films

The thermo-oxidative degradation of EVA- and EBA-based nanocomposites was evaluated through TGA analyses in an oxidative atmosphere; the obtained curves are depicted in Figure 1, while the main results are listed in Table 1. Unfilled EVA (Figure 1A) undergoes three degradation steps. According to the literature [16,32], the first step, occurring between 290 and 390 °C, is associated with the evolution of acetic acid. The second stage (occurring between 400 and 470 °C) is attributed to the decomposition of the ethylene-co-acetylene random copolymer resulting from deacylation. Finally, for 490 to 580 °C, the oxidation of the products formed during the previous steps occurs. Also, for EBA (Figure 2B), three main degradation stages can be identified [22,33]. In this case, the first step (250–340 °C) is associated with the cleavage of the butyl acrylate chains, the second one (340–430 °C) is attributed to the chain scission of the polymer backbone and further oxidation of the

previously formed unsaturated fragments, and the last decomposition step involves the oxidation of the remaining residue.

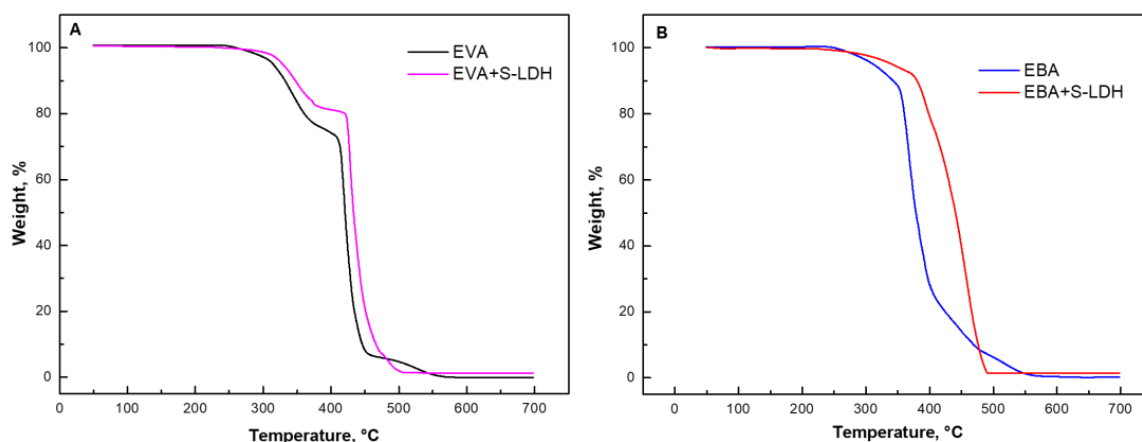


Figure 1. TGA curves for frequency for (A) EVA- and (B) EBA-based materials containing S-LDHs.

Table 1. Main results of TGA analyses performed in air.

	T_{onset} [°C]	T_{max} [°C]	Residue @ 600 °C [%]
EVA	291.2	419.7	0
EVA + S-LDHs	310.3	428.9	1.44
EBA	281.5	367.0	0
EBA + S-LDHs	294.8	422.7	1.53

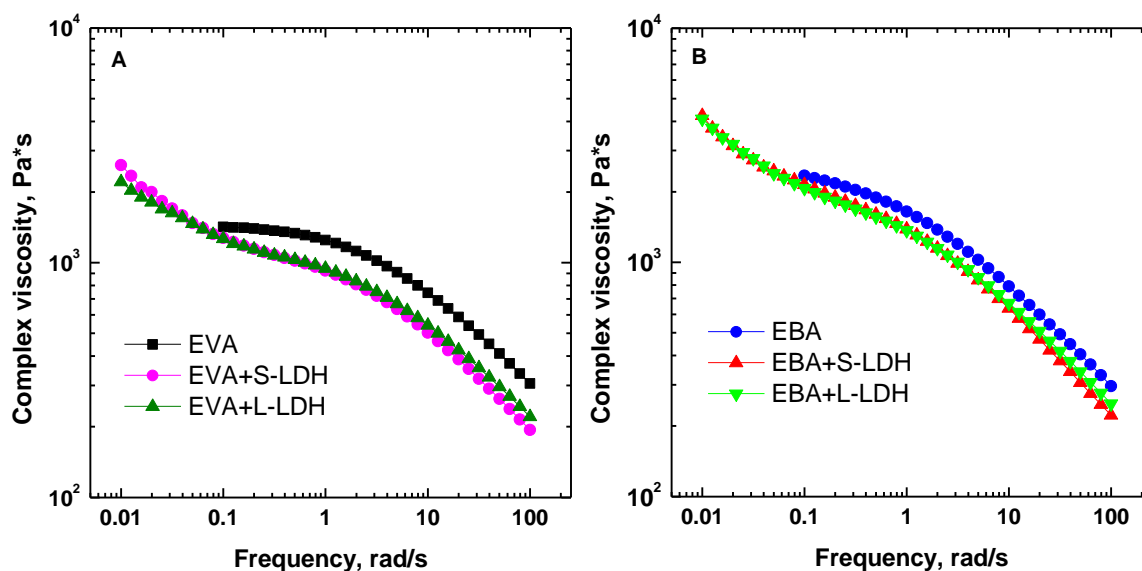


Figure 2. Complex viscosity curves as a function of the frequency for (A) EVA- and (B) EBA-based materials.

The incorporation of both types of LDHs (the results for the films containing S-LDH are reported in Figure 1A,B and Table 1) results in an enhancement of the thermo-oxidative resistance of both copolymers. Specifically, the EVA-based nanocomposite exhibits an increase in both T_{onset} and T_{max} compared to the unfilled matrix. The effect of the nanofillers is even more considerable for EBA+S-LDHs, as highlighted by an increase of approximately 14 °C in T_{onset} and of 55 °C in T_{max} with respect to the neat copolymer. As widely reported

in the literature, the observed delay in the thermo-oxidative phenomena of the nanocomposites can be attributed to the barrier to oxygen and to the volatile degradation products generated by the embedded nanofillers, as well as to their thermal insulating action [34–36].

Table 2 presents the main results of the thermal characterization of the nanocomposite films. The thermograms recorded during the first heating scan are reported in Figures S1 and S2. According to the literature [37], both pristine copolymers show two melting peaks, corresponding to the primary and secondary crystallization. From a general point of view, the introduction of the nanofillers does not significantly affect the melting temperatures of the unfilled matrices or the crystallinity content.

Table 2. Melting temperatures and crystallinity content for EVA- and EBA-based nanocomposite films.

	T_{m1} [°C]	T_{m2} [°C]	χ_c [%]
EVA	48	81	32
EVA + S-LDHs	48	85	31
EVA + L-LDHs	49	83	31
EBA	50	94	36
EBA + S-LDHs	51	94	34
EBA + L-LDHs	51	96	35

The complex viscosity curves as a function of the frequency obtained through frequency sweep tests are reported in Figure 2A,B. Both copolymers show the expected pseudo-plastic trend, involving the appearance of a Newtonian plateau in the low-frequency region, followed by a shear-thinning behavior at high frequencies. It should be noted that EBA, especially at low frequencies, shows higher viscosity values than EVA and less pronounced Newtonian characteristics, likely due to the different molecular weights of the two copolymers. The incorporation of the nanofillers causes the disappearance of the Newtonian plateau in the low-frequency region; in fact, all the investigated nanocomposite films exhibit a yield stress behavior, associated with the establishment of copolymer–filler and filler–filler interactions that hinder the complete relaxation of the copolymer macromolecules [38].

Looking at the high-frequency region, lower complex viscosity values are obtained for the nanocomposite films compared to the unfilled copolymers. According to the literature [39], this behavior can be explained by considering a preferential orientation of the nanofillers along the shear flow direction. Lastly, it should be noted that the different aspect ratios of the LDHs do not affect the rheological response of the nanocomposites. In fact, for both EVA- and EBA-based systems, practically overlapping viscosity curves are obtained as a result of the incorporation of S-LDHs or L-LDHs.

From the SEM micrographs shown in Figure 3, it is evident that, regardless of matrix and type of filler, the lamellar nanofillers appear, in general, well dispersed and well distributed. In fact, in both matrices, the nanofillers are mainly dispersed as thin platelets with a thickness of less than a micrometer. Furthermore, a clear, strong orientation of the nanofillers in the direction of the production of the films (i.e., machine direction) can be observed, mainly attributable to the application of the non-isothermal elongation flow during the cast extrusion and calendaring processes.

However, although rheological analyses suggested an excellent extent of dispersion/distribution of the nanofillers in both matrices, it should be noted that EBA-based nanocomposites exhibit the presence of some large-sized aggregates, as illustrated in the micrograph presented in Figure 4. Thus, it seems that the LDHs dispersion in EBA is less effective than in EVA, likely because of the different polarity of the copolymers. In

particular, owing to the presence of butyl groups, EBA is less polar compared to EVA, making this copolymer less compatible with the embedded nanofillers.

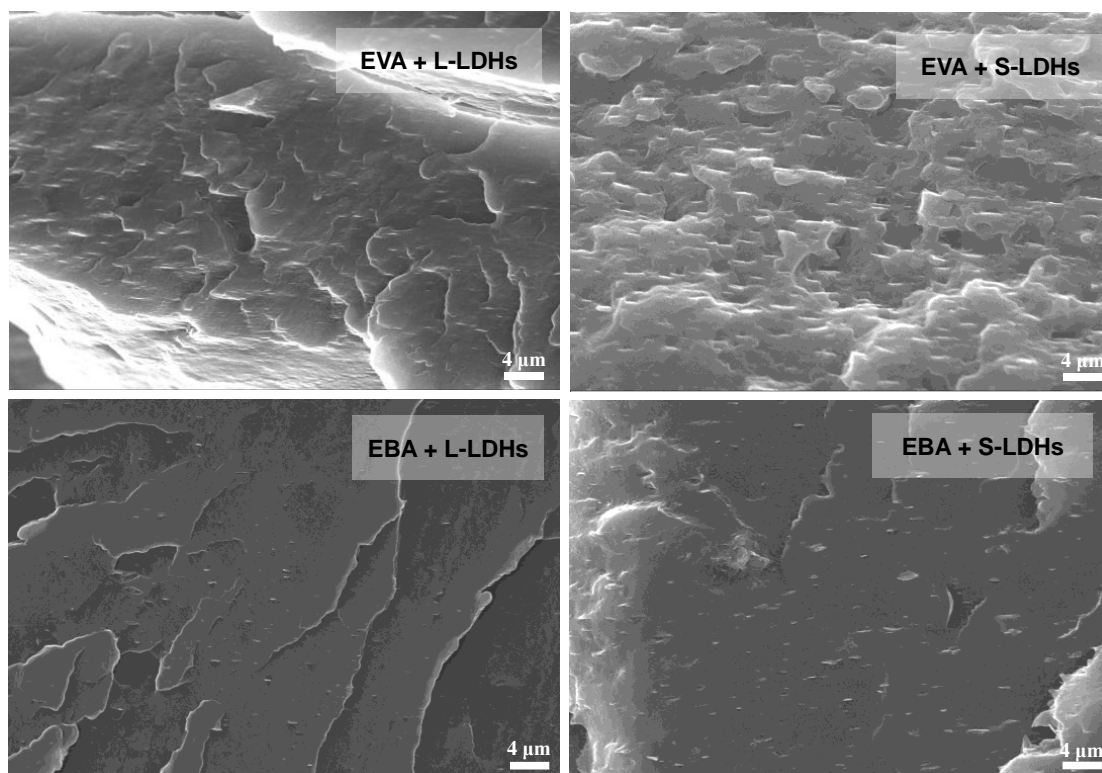


Figure 3. SEM micrographs for EVA- and EBA-based nanocomposite films.

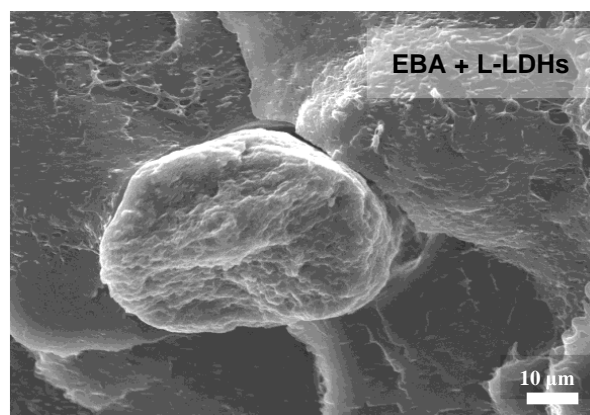


Figure 4. SEM micrographs of EBA-based nanocomposite film containing L-LDHs showing a nanofiller aggregate.

3.2. Combustion Behavior of Coated Samples

As already illustrated in the experimental section, the EVA- and EBA-based films were applied to compression-molded specimens of pristine copolymers through a further compression molding process, and the combustion behavior of the so-obtained coated samples was evaluated through cone calorimeter tests with an incident heat flux of 30 kW/m². The obtained curves of HRR as a function of time for uncoated and surface-coated samples are reported in Figure 5A,B for EVA- and EBA-based materials, respectively. Additionally, THR curves are depicted in Figures S3 and S4, and Table 3 reports the most relevant data and parameters collected during these tests.

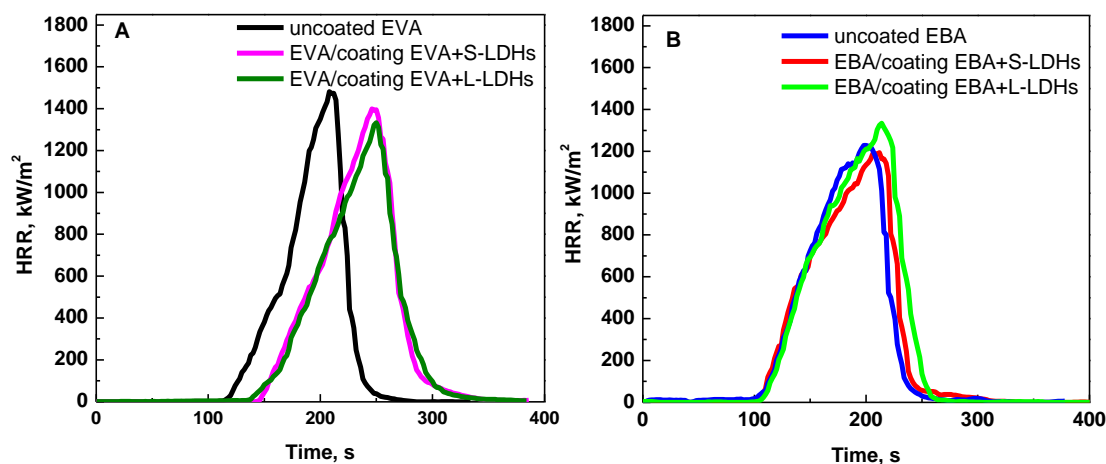


Figure 5. HRR as a function of time: cone calorimetry (heat flux = 30 kW/m²) curves of (A) EVA- and (B) EBA-coated samples. The curves for uncoated EVA and EBA specimens are also reported.

Table 3. Cone calorimetry (heat flux = 30 kW/m²) data and parameters of all investigated coated samples and pristine copolymers.

	TTI [s]	TTP [s]	FPI [m ² s/kW]	FIGRA [kW/m ² s]
EVA	101 ± 1	210 ± 2	0.0675 ± 0.0027	7.1 ± 0.3
EVA/coating EVA + S-LDHs	133 ± 3	252 ± 6	0.0910 ± 0.0015	5.8 ± 0.1
EVA/coating EVA + L-LDHs	135 ± 13	255 ± 5	0.0968 ± 0.0119	5.5 ± 0.2
EBA	91 ± 5	194 ± 12	0.0749 ± 0.0053	6.3 ± 0.5
EBA/coating EBA + S-LDHs	102 ± 2	208 ± 4	0.0836 ± 0.0036	5.9 ± 0.2
EBA/coating EBA + L-LDHs	107 ± 3	214 ± 2	0.0848 ± 0.0068	5.9 ± 0.3

Concerning EVA-based samples, it is evident that the application of surface coatings results in a significant delay in the ignition of the specimens. This phenomenon can be noticed by looking at the HRR curves of the coated specimens, which are shifted forward by about 30 s, irrespective of the type of LDHs. Furthermore, the shape of the curves remains almost unchanged compared to that of the uncoated EVA sample. In fact, once the protective action of the surface coating is exhausted, the underlying pure EVA specimen undergoes almost complete combustion, resulting in a negligible final residue.

The increase in TTI for samples coated with a surface film containing nanoclays has already been reported in the literature [9,40,41]. In particular, it has been demonstrated that during the heating of the material, the ablation of polymer chains promotes the migration of the lamellae towards the surface to form a physical ceramic barrier that limits the heat and oxygen fluxes towards the underlying polymer. Concurrently, the coating also acts as a barrier for the volatile gases resulting from the thermal degradation of the underlying polymer. It has been established that, due to the low thickness of the barrier layer and the minimal filler content, its protective efficacy is restricted to the early stage of the cone calorimeter test. In fact, due to the increasing pressure of volatiles produced by the substrate, the rupture of the film occurs, and the process proceeds through the ignition of the gas phase and the subsequent combustion of the polymer, with the same mechanism as uncoated materials. However, it should be noticed that the surface localization of the nanofillers on the polymer surface has a beneficial effect on TTI with respect to the classical bulk incorporation. In fact, in this last case, an anticipation of ignition is often observed compared to unfilled polymers [42].

In contrast, for EBA-coated samples, a less relevant delay in TTI is observed. This result can be explained by considering the poorer dispersion of the LDH nanoparticles

in this copolymer compared to EVA, as assessed through morphological analyses. In particular, the presence of LDH aggregates in EBA results in a reduced number of mobile lamellae available to form the physical barrier in close proximity to the specimen surface [41]. Furthermore, the different TTI of the two uncoated copolymers should also be considered; in particular, the results of the cone calorimeter tests demonstrate that the ignition is anticipated for EBA compared to EVA. Therefore, the different effectiveness of the surface coating in the two cases can also be explained by the fact that, under a heat flux of 30 kW/m^2 , the rate at which the LDHs lamellae arrange to form the protective layer is lower than the EBA ignition. In order to verify a possible protective effect of the surface coating also for EBA-based systems, the cone calorimeter tests were also performed at a lower heat flux, namely 25 kW/m^2 . Due to the lower thermal power transmitted to the specimen, the time required to reach ignition temperature is extended [43], thereby enabling the protective action of the coating to be manifested.

Figure 6 shows the HRR curves of EBA-based samples under a heat flux of 25 kW/m^2 , while Table 4 summarizes the main results and parameters (THR curves are reported in Figure S5). It can be clearly observed that, in this case, the surface-coated samples exhibit delayed TTI compared to the uncoated EBA. In this fire scenario (namely, at low heat flux), the thermo-oxidative degradation of EBA is slowed down; in fact, the TTI is 30% higher than at 30 kW/m^2 . Therefore, the LDH lamellae have the capacity to organize themselves in order to form a protective layer, thereby promoting the ignition delay.

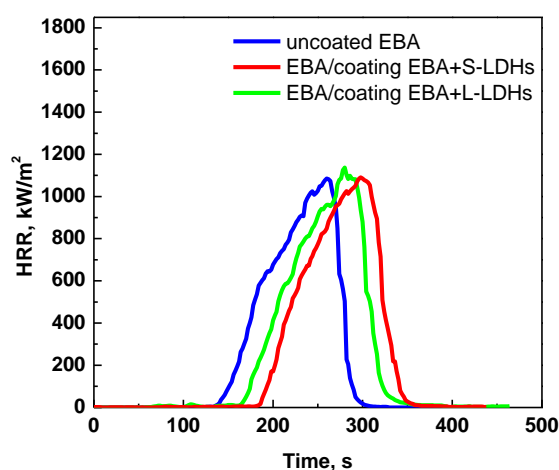


Figure 6. HRR as a function of time: cone calorimetry (heat flux = 25 kW/m^2) curves of uncoated EBA and EBA-based surface-coated samples.

Table 4. Cone calorimetry (heat flux = 25 kW/m^2) data and parameters of uncoated and surface-coated EBA-based samples.

	TTI [s]	TTP [s]	FPI [$\text{m}^2\text{s/kW}$]	FIGRA [$\text{kW/m}^2\text{s}$]
EBA	124 ± 4	242 ± 9	0.1137 ± 0.0008	4.5 ± 0.4
EBA/coating EBA + S-LDHs	173 ± 9	307 ± 3	0.1470 ± 0.0200	3.9 ± 0.4
EBA/coating EBA + L-LDHs	161 ± 5	268 ± 9	0.1416 ± 0.0031	4.2 ± 0.1

Apart from the differences in TTI, for all investigated samples, the shape of the HRR curve remains almost unchanged compared to that of the uncoated copolymer. The THR of EVA and EBA/coating is higher with respect to the corresponding neat polymers due to the fact that the coated samples contain a higher amount of polymer. Additionally, it can be observed that, regardless of the copolymer matrix, the surface-coated samples show increased FPI and decreased FIGRA with respect to the corresponding uncoated substrates

(see values reported in Tables 3 and 4), basically due to the increase in TTI discussed earlier, indicating better performance in the evaluated scenarios.

4. Conclusions

In this work, a surface-coating approach for imparting flame retardancy to ethylene-based copolymers is proposed. Specifically, films based on EVA and EBA and containing two types of LDHs were firstly prepared through cast extrusion and then applied through compression molding to the corresponding matrix substrates. The preliminary characterization of the films highlighted the achievement of a homogeneous dispersion and distribution of the embedded nanofillers (which also appeared preferentially oriented along the machine direction) regardless of the matrix and notwithstanding the presence of some aggregates in EBA-based materials. Cone calorimeter tests at high heat flux (i.e., 30 kW/m²) demonstrated the effectiveness of the surface coating in delaying the time to ignition of EVA-based materials. For EBA-based coated samples, a less evident increase in TTI compared to the uncoated sample was observed. This result can be explained by considering two different aspects. Firstly, the lower polarity of EBA with respect to EVA resulted in poorer dispersion of the embedded nanofillers, making it more difficult to form the protective layer. On the other hand, the protective action of the coating was also hindered by the anticipated ignition of EBA, which hampered the organization of the dispersed LDH lamellae in a protective layer. To confirm this last assumption, for the EBA-based material, the cone calorimeter test was repeated at a lower heat flux (namely, 25 kW/m²). In this scenario, the slower thermo-degradation of the copolymer allowed the dispersed nanofillers to rearrange and form a more efficient protective shield, resulting in delayed ignition. Overall, the proposed coating strategy represents a promising and versatile approach to enhance the surface flame retardancy of EVA- and EBA-based systems. In particular, this methodology can be effectively exploited for the protection of cables and wires, which are commonly formulated using EVA or EBA as base polymers, providing improved fire performance without significantly altering the bulk properties or processability of the materials.

Supplementary Materials: The following supporting information can be downloaded at <https://www.mdpi.com/article/10.3390/polym17233189/s1>. Figure S1: DSC thermograms collected during the first heating scan for unfilled EVA and EVA-based nanocomposite films. Figure S2: DSC thermograms collected during the first heating scan for unfilled EBA and EBA-based nanocomposite films. Figure S3: THR curves for EVA and EVA-based specimens (heat flux = 30 kW/m²). Figure S4: THR curves for EBA and EBA-based specimens (heat flux = 30 kW/m²). Figure S5: THR curves for EBA and EBA-based specimens (heat flux = 25 kW/m²).

Author Contributions: Conceptualization, A.F. and R.A.; methodology, A.F., R.A. and M.S.; validation, A.F. and M.B.; formal analysis, G.T. and M.B.; investigation, G.T. and M.S.; writing—original draft preparation, G.T.; writing—review and editing, R.A. and A.F.; supervision, A.F. All authors have read and agreed to the published version of the manuscript.

Funding: This research received no external funding.

Institutional Review Board Statement: Not applicable.

Data Availability Statement: Dataset available on request from the authors.

Acknowledgments: The authors thank Günter Beyer for fruitful discussion and Lucobit for supplying the materials.

Conflicts of Interest: The authors declare no conflicts of interest.

References

1. Laoutid, F.; Bonnaud, L.; Alexandre, M.; Lopez-Cuesta, J.M.; Dubois, P. New prospects in flame retardant polymer materials: From fundamentals to nanocomposites. *Mater. Sci. Eng. R Rep.* **2009**, *63*, 100–125.
2. Wu Klingler, W.; Rougier, V.; Huang, Z.; Parida, D.; Lehner, S.; Casutt, A.; Gaan, S. Recyclable flame retardant phosphonated epoxy based thermosets enabled via a reactive approach. *Chem. Eng. J.* **2023**, *466*, 143051. [\[CrossRef\]](#)
3. Hornsby, P.R. Fire retardant fillers for polymers. *Int. Mater. Rev.* **2001**, *46*, 199–210. [\[CrossRef\]](#)
4. Silva, N.G.S.; Zanini, N.C.; De Souza, A.G.; Barbosa, R.F.S.; Rosa, D.S.; Mulinari, D.R. *Halogen-Based Flame Retardants in Polyurethanes*; American Chemical Society: Washington, DC, USA, 2021; Volume 1399, pp. 141–171.
5. Kaspersma, J.; Doumen, C.; Munro, S.; Prins, A.M. Fire retardant mechanism of aliphatic bromine compounds in polystyrene and polypropylene. *Polym. Degrad. Stab.* **2002**, *77*, 325–331. [\[CrossRef\]](#)
6. Chen, L.; Wang, Y.Z. Aryl polyphosphonates: Useful halogen-free flame retardants for polymers. *Materials* **2010**, *3*, 4746–4760. [\[CrossRef\]](#)
7. Camino, G.; Costa, L.; Luda, M.P. Mechanistic aspects of intumescent fire-retardant systems. *Makromol. Chem. Macromol. Symp.* **1993**, *74*, 71–83. [\[CrossRef\]](#)
8. Camino, G.; Costa, L.; Martinasso, G. Intumescent fire-retardant systems. *Polym. Degrad. Stab.* **1989**, *23*, 359–376. [\[CrossRef\]](#)
9. Porter, D.; Metcalfe, E.; Thomas, M.J.K. Nanocomposite fire retardants—A review. *Fire Mater.* **2000**, *24*, 45–52. [\[CrossRef\]](#)
10. Lorenzi, E.; Arrigo, R.; Frache, A. Development of a Polypropylene-Based Material with Flame-Retardant Properties for 3D Printing. *Polymers* **2024**, *16*, 858.
11. Peng, Y.; Niu, M.; Qin, R.; Xue, B.; Shao, M. Study on flame retardancy and smoke suppression of PET by the synergy between Fe₂O₃ and new phosphorus-containing silicone flame retardant. *High Perform. Polym.* **2020**, *32*, 936–948. [\[CrossRef\]](#)
12. Liu, Y.; Gao, Y.; Wang, Q.; Lin, W. The synergistic effect of layered double hydroxides with other flame retardant additives for polymer nanocomposites: A critical review. *Dalton Trans.* **2018**, *47*, 14827–14840. [\[CrossRef\]](#)
13. Shea, J.J. Handbook of Building Materials for Fire Protection [Book Review]. *IEEE Electr. Insul. Mag.* **2004**, *20*, 66. [\[CrossRef\]](#)
14. Feng, C.; Liang, M.; Chen, W.; Huang, J.; Liu, H. Flame retardancy and thermal degradation of intumescent flame retardant EVA composite with efficient charring agent. *J. Anal. Appl. Pyrolysis* **2015**, *113*, 266–273. [\[CrossRef\]](#)
15. Bourbigot, S.; Le Bras, M.; Leeuwendal, R.; Shen, K.K.; Schubert, D. Recent advances in the use of zinc borates in flame retardancy of EVA. *Polym. Degrad. Stab.* **1999**, *64*, 419–425. [\[CrossRef\]](#)
16. Camino, G.; Sgobbi, R.; Zaopo, A.; Colombier, S.; Scelza, C. Investigation of flame retardancy in EVA. *Fire Mater.* **2000**, *24*, 85–90. [\[CrossRef\]](#)
17. Ye, L.; Qu, B. Flammability characteristics and flame retardant mechanism of phosphate-intercalated hydrotalcite in halogen-free flame retardant EVA blends. *Polym. Degrad. Stab.* **2008**, *93*, 918–924. [\[CrossRef\]](#)
18. Xu, B.; Ma, W.; Wu, X.; Qian, L.; Jiang, S. Flame retardancy and thermal behavior of intumescent flame-retardant EVA composites with an efficient triazine-based charring agent. *Mater. Res. Express* **2018**, *5*, 045309. [\[CrossRef\]](#)
19. Camino, G.; Maffezzoli, A.; Braglia, M.; De Lazzaro, M.; Zapparano, M. Effect of hydroxides and hydroxycarbonate structure on fire retardant effectiveness and mechanical properties in ethylene-vinyl acetate copolymer. *Polym. Degrad. Stab.* **2001**, *74*, 457–464. [\[CrossRef\]](#)
20. Zhang, H.; Wang, H.; Wang, H. Flame retardant mechanism and surface modification of magnesium hydroxide flame retardant. *IOP Conf. Ser. Earth Environ. Sci.* **2018**, *170*, 032028. [\[CrossRef\]](#)
21. Ramazani, S.A.A.; Rahimi, A.; Frounchi, M.; Radman, S. Investigation of flame retardancy and physical-mechanical properties of zinc borate and aluminum hydroxide propylene composites. *Mater. Des.* **2008**, *29*, 1051–1056.
22. Huang, N.; Wang, J. A TGA-FTIR study on the effect of CaCO₃ on the thermal degradation of EBA copolymer. *J. Anal. Appl. Pyrolysis* **2009**, *84*, 124–130.
23. Tademr, M.; Yildirim, H. Thermal degradation studies of different polar polyethylene copolymers. *J. Appl. Polym. Sci.* **2002**, *84*, 1465–1473. [\[CrossRef\]](#)
24. Moyano, M.A.; París, R.; Martín-Martínez, J.M. Viscoelastic and adhesion properties of hot-melts made with blends of ethylene-co-n-butyl acrylate (EBA) and ethylene-co-vinyl acetate (EVA) copolymers. *Int. J. Adhes. Adhes.* **2019**, *88*, 34–42. [\[CrossRef\]](#)
25. Ellis, T.S.; D'Angelo, J.S. Thermal and mechanical properties of a polypropylene nanocomposite. *J. Appl. Polym. Sci.* **2003**, *90*, 1639–1647. [\[CrossRef\]](#)
26. Colonna, S.; Cuttica, F.; Frache, A. Aging of EVA/organically modified clay: Effect on dispersion, distribution and combustion behavior. *Polym. Degrad. Stab.* **2014**, *107*, 184–187. [\[CrossRef\]](#)
27. Malucelli, G.; Carosio, F.; Alongi, J.; Fina, A.; Frache, A.; Camino, G. Materials engineering for surface-confined flame retardancy. *Mater. Sci. Eng. R Rep.* **2014**, *84*, 1–20. [\[CrossRef\]](#)
28. Matta, S.; Bartoli, M.; Arrigo, R.; Frache, A.; Malucelli, G. Flame retardant potential of Tetra Pak[®]-derived biochar for ethylene-vinyl-acetate copolymers. *Compos. Part C Open Access* **2022**, *8*, 100252.

29. Arrigo, R.; Frache, A. FDM Printability of PLA Based-Materials: The Key Role of the Rheological Behavior. *Polymers* **2022**, *14*, 1754. [[CrossRef](#)]
30. Schartel, B.; Hull, T.R. Development of fire-retarded materials—Interpretation of cone calorimeter data. *Fire Mater.* **2007**, *31*, 327–354.
31. Hirschler, M.M. Use of heat release rate to predict whether individual furnishings would cause Self propagating fires. *Fire Saf. J.* **1999**, *32*, 273–296. [[CrossRef](#)]
32. Riva, A.; Zanetti, M.; Braglia, M.; Camino, G.; Falqui, L. Thermal degradation and rheological behaviour of EVA/montmorillonite nanocomposites. *Polym. Degrad. Stab.* **2002**, *77*, 299–304. [[CrossRef](#)]
33. Sultan, B.; Sörvik, E. Thermal degradation of EVA and EBA—A comparison. I. Volatile decomposition products. *J. Appl. Polym. Sci.* **1991**, *43*, 1737–1745. [[CrossRef](#)]
34. Wang, X.; Rathore, R.; Songtipya, P.; Jimenez-Gasco, M.; Manias, E.; Wilkie, C.A. EVA-layered double hydroxide (nano)composites: Mechanism of fire retardancy. *Polym. Degrad. Stab.* **2011**, *96*, 301–313. [[CrossRef](#)]
35. Karimpour-Motlagh, N.; Khonakdar, H.A.; Jafari, S.M.A.; Mahjub, A.; Panahi-Sarmad, M.; Kasbi, S.F.; Shojaei, S.; Goodarzi, V.; Arjmand, M. Influence of polypropylene and nanoclay on thermal and thermo-oxidative degradation of poly(lactic acid): TG-FTIR, TG-DSC studies and kinetic analysis. *Thermochim. Acta* **2020**, *691*, 178709. [[CrossRef](#)]
36. Golebiewski, J.; Galeski, A. Thermal stability of nanoclay polypropylene composites by simultaneous DSC and TGA. *Compos. Sci. Technol.* **2007**, *67*, 3442–3447. [[CrossRef](#)]
37. Stark, W.; Jaunich, M. Investigation of Ethylene/Vinyl Acetate Copolymer (EVA) by thermal analysis DSC and DMA. *Polym. Test.* **2011**, *30*, 236–242. [[CrossRef](#)]
38. Arrigo, R.; Ronchetti, S.; Montanaro, L.; Malucelli, G. Effects of the nanofiller size and aspect ratio on the thermal and rheological behavior of PEG nanocomposites containing boehmites or hydrotalcites. *J. Therm. Anal. Calorim.* **2018**, *134*, 1667–1680. [[CrossRef](#)]
39. Chandran, N.; Sarathchandran, C.; Thomas, S. Rheology of polymer-clay nanocomposites. In *Rheology of Polymer Blends and Nanocomposites: Theory, Modelling and Applications*; Elsevier: Amsterdam, The Netherlands, 2019; pp. 97–122.
40. Hornsby, P.R.; Rotheron, R.N.; Takeda, K.; Pelegris, C.; Kashiwagi, T.; Lomakin, S.; Georlette, P. Use of Nanocomposite Materials: Flammability of Nanocomposites: Effects of the Shape of Nanoparticles. In *Fire Retardancy of Polymers*; The Royal Society of Chemistry: Cambridge, UK, 2007; pp. 79–99.
41. Camino, G.; Tartaglione, G.; Frache, A.; Manfredi, C.; Costa, G. Thermal and combustion behaviour of layered silicate-epoxy nanocomposites. *Polym. Degrad. Stab.* **2005**, *90*, 354–362. [[CrossRef](#)]
42. Fina, A.; Camino, G. Ignition mechanisms in polymers and polymer nanocomposites. *Polym. Adv. Technol.* **2011**, *22*, 1147–1155. [[CrossRef](#)]
43. Fina, A.; Cuttica, F.; Camino, G. Ignition of polypropylene/montmorillonite nanocomposites. *Polym. Degrad. Stab.* **2012**, *97*, 2619–2626. [[CrossRef](#)]

Disclaimer/Publisher’s Note: The statements, opinions and data contained in all publications are solely those of the individual author(s) and contributor(s) and not of MDPI and/or the editor(s). MDPI and/or the editor(s) disclaim responsibility for any injury to people or property resulting from any ideas, methods, instructions or products referred to in the content.